An Investigation of New FETD/ABC Methods of Computation of Scattering from Three-Dimensional Material Objects

Kenneth S. Komisarek, Nan N. Wang, Allen K. Dominek, and Raiford Hann

***Abstract*—Finite-element time-domain (FETD) and absorbing boundary condition (ABC) methods for computation of scattering from three-dimensional (3-D) material objects are developed and investigated. The methods involve discrete-time FETD solution of the time-domain Helmholtz equation in a region that comprises the 3-D scatterer and its immediate vicinity. Coupling of the solution to the surrounding infinite space is achieved through the ABC. This FETD/ABC formulation is examined for a number of various geometries: sphere, plate, and ogive.**

I. Introduction

SINCE the introduction of the finite-element method (FEM) to the arena of computational electromagnetics, it has been almost exclusively limited to its use in finite-element frequency-domain (FEFD) methods. Up until recent times, finite-difference time-domain (FDTD) [1] was employed almost exclusively for time-domain scattering problems. Only in recent times have finite-element formulations been developed for the time domain [2]–[4]. The primary reason for the recent interest in the time domain with regards to finite elements [5] is that of possible gains in computational efficiency, especially in regard to economizing central processing unit (CPU) time. Barring the development of faster computers, the only way to achieve a decrease in time spent on complex electromagnetic scattering calculation is to devise new and more time-efficient methods of solution. Hence, the development and investigation of three-dimensional (3-D) finite-element time-domain (FETD) methods is chronicled here.

FETD reduces a scattering problem into a matrix of real constant coefficient nonhomogeneous differential equations, with time as the independent variable and a vector of electromagnetic field coefficients as the set of dependent variables. These field coefficients are decoupled from the geometric quantities that describe the scatterer (i.e., position, shape, composition) since it is assumed that the scatterer geometry does not change with time. All of the geometric information about the scatterer, as well as its coupling to the surrounding space, is incorporated into the matrices of real constant coefficients. The electromagnetic wave that illuminates the scatterer is incorporated into a real excitation vector, thus making the differential equation system nonhomogeneous. The field coefficients for a particular excitation are found by discretely integrating forward or stepping the differential equation system in time. Near and far fields can then be found from the time history of the field coefficients.

The earliest finite-element formulations were developed for bounded problems such as waveguides and cavities [6], [7]. An unbounded scattering problem requires coupling of the scatterer and its immediate vicinity to the surrounding unbounded region. In the literature, this coupling has been accomplished chiefly by three methods, the perfectly matched layer (PML) [8], [9], the boundary-element method (BEM) [10], [11], and the absorbing boundary condition (ABC) [12]–[14]. The ABC method has been chosen here because of simplicity. A FETD formulation with a simple first-order Sommerfeld-type ABC has been developed by Ali and Costache [15] and also used by Mahadevan and Mittra [16]. Mahadevan and Mittra employed two coupled Maxwell's curl equations in their FETD formulation. Presented in this work is a Helmholtz equation based FETD formulation involving a second-order ABC.

The paper is based on the work of Komisarek [17] and is organized as follows. Section II presents the basic FETD matrix equation. Section III presents the second-order ABC coupling. Two time-stepping methods employed to integrate the resulting FETD matrix equations are outlined in Section IV. The results of some computations involving the new FETD methods are presented in Section V. Some concluding remarks are given in Section VI.

II. FETD Formulation

The FETD formulation begins with Maxwell's curl equations in space-time R^4 for isotropic inhomogeneous media given by

$$\nabla \times \mathcal{E} = -\mu' \frac{\partial \mathcal{H}}{\partial t} - \sigma_m \mathcal{H} \tag{1}$$

and

$$\nabla \times \mathcal{H} = \epsilon' \frac{\partial \mathcal{E}}{\partial t} + \sigma_e \mathcal{E} \tag{2}$$

Manuscript received December 29, 1997; revised March 17, 1999.

K. S. Komisarek and N. N. Wang were with the ElectroScience Laboratory, Department of Electrical Engineering, The Ohio State University, Columbus, OH 43212 USA. They are now with the Raytheon Systems Company Radar Design Center, Sudbury, MA USA.

A. K. Dominek was with the ElectroScience Laboratory, Department of Electrical Engineering, The Ohio State University, Columbus, OH 43212 USA. He is now with Analytic Designs, Inc., Columbus, OH 43215 USA.

R. Hann was with the Computational Material Laboratory, Material Division, National Aeronautics and Space Administration, Cleveland, OH 44111 USA. He is now with the Raytheon Systems Company Radar Design Center, Sudbury, MA USA.

Publisher Item Identifier S 0018-926X(99)09389-8.

where ϵ' is the permittivity, μ' is the permeability, σ_e is the electrical conductivity, and σ_m is the magnetic conductivity. The relationships between these four quantities and the frequency-domain complex permittivity ϵ and complex permeability μ are given by

$$\epsilon = \epsilon' - j\frac{\sigma_e}{\omega} \tag{3}$$

and

$$\mu = \mu' - j\frac{\sigma_m}{\omega} \tag{4}$$

where ω is the time-harmonic radian frequency and the $e^{j\omega t}$ time convention is assumed wherever the frequency domain is involved.

Elimination of the magnetic field in (1) and (2) yields the following double curl or vector Helmholtz equation:

$$\nabla \times \frac{1}{\mu'}\nabla \times \mathcal{E} + \epsilon'\frac{\partial^2 \mathcal{E}}{\partial t^2} + \left[\sigma_e + \frac{\epsilon'}{\mu'}\sigma_m\right]\frac{\partial \mathcal{E}}{\partial t} + \frac{\sigma_e \sigma_m}{\mu'}\mathcal{E} = 0 \text{ in } V. \tag{5}$$

V is a volume that contains the scatterer and some of the free-space surrounding the scatterer. V is bounded by a surface S that exists completely in free-space and is not in contact with the scatterer. S is called the truncation boundary. Equation (5) is weakened throughout V via weighting with a vector function $\mathbf{v}_m$ as follows:

$$\int_V \mathbf{v}_m \cdot \left(\nabla \times \frac{1}{\mu'}\nabla \times \mathcal{E} + \epsilon'\frac{\partial^2 \mathcal{E}}{\partial t^2} + \left[\sigma_e + \frac{\epsilon'}{\mu'}\sigma_m\right]\frac{\partial \mathcal{E}}{\partial t} + \frac{\sigma_e \sigma_m}{\mu'}\mathcal{E}\right) dV = 0. \tag{6}$$

Within V, all of space is meshed into tetrahedral elements. The material in each element is homogeneous. Additionally, resistive card and PEC surfaces may reside on the triangular interfaces between the elements. Each triangular resistive or PEC surface is associated with one of its two adjoining elements. The electric field throughout V is expanded in terms of N vector basis functions as follows:

$$\mathcal{E} = \sum_{n=1}^{N} e_n(t)\mathbf{w}_n \tag{7}$$

where the time-independent $\mathbf{w}_n$ are the linear edge-based vector expansion functions of [19] and the $e_n(t)$ are their corresponding time-varying expansion coefficients, one for each of the N edges of the mesh not on a PEC surface. The particular edge-based vector expansion employed in (7) has been chosen since it is not plagued by the spurious contributions or nonphysical resonances in the solution that are characteristic of nodal-based expansions [20].

Application of vector identities, one of Gauss' theorems, time-domain resistive boundary conditions, the expansion of (7), and the choice of N testing functions $\mathbf{v}_m = \mathbf{w}_m$, results in the FETD matrix equation

$$\mathbf{T_F}\frac{d^2}{dt^2}\mathbf{e}(t) + \mathbf{R_F}\frac{d}{dt}\mathbf{e}(t) + \mathbf{S_F}\mathbf{e}(t) = \mathbf{f}(t) \tag{8}$$

where the elements of the finite-element matrices are given by

$$T_{F_{m,n}} = \int_V \epsilon' \mathbf{w}_m \cdot \mathbf{w}_n \, dV \tag{9}$$

$$R_{F_{m,n}} = \int_V \left(\sigma_e + \frac{\epsilon'}{\mu'}\sigma_m\right)\mathbf{w}_m \cdot \mathbf{w}_n \, dV + \int_S R^{-1}(\hat{n} \times \mathbf{w}_m) \cdot (\hat{n} \times \mathbf{w}_n) \, dS \tag{10}$$

$$S_{F_{m,n}} = \int_V \frac{1}{\mu'}(\nabla \times \mathbf{w}_m) \cdot (\nabla \times \mathbf{w}_n) \, dV + \int_V \frac{\sigma_e \sigma_m}{\mu'}\mathbf{w}_m \cdot \mathbf{w}_n \, dV \tag{11}$$

where R is the resistance sheet resistivity and the elements of the excitation vector are given by

$$f_m(t) = -\frac{1}{\mu_\circ}\int_S \mathbf{w}_m \cdot (\hat{n} \times \nabla \times [\mathcal{E}^i + \mathcal{E}^s]) \, dS \tag{12}$$

for $m = 1, \cdots N$ and $n = 1, \cdots, N$, where $\mathcal{E}^i$ is the incident electric field and $\mathcal{E}^s$ is the scattered electric field. Since the weighting and expansion functions are the same, this is a Galerkin formulation. The dependence of the integral in (12) is eliminated through the use of the ABC presented in the next section.

III. Absorbing Boundary Conditions

The ABC employed on the truncation boundary S is a time-domain version of the frequency domain second-order ABC of Webb *et al.* [13] given by

$$\hat{n} \times \nabla \times \mathbf{E}^s = j\omega c_\circ^{-1}\mathbf{E}_t^s + \gamma(r)\nabla \times [\hat{n}(\hat{n} \cdot \nabla \times \mathbf{E}^s)] + (s-1)\gamma(r)\nabla_t(\nabla \cdot \mathbf{E}_t^s) + (2-s)j\omega c_\circ^{-1}\beta(r)\nabla_t(\hat{n} \cdot \mathbf{E}^s) \tag{13}$$

where

$$\gamma(r) = \frac{c_\circ/2}{j\omega + c_\circ/r} \tag{14}$$

r is the local radius of curvature of the truncation boundary, $c_\circ$ is the speed of light in free-space, and s is a scalar parameter. The subscript t denotes the transverse vector component. In the interest of preserving the symmetry of the matrices of the final form of the FETD formulation, s is set equal to two in (13). Fourier transform theory yields the time domain analog of (13) given by

$$\hat{n} \times \nabla \times \mathcal{E}^s = \frac{1}{c_\circ}\frac{\partial}{\partial t}\mathcal{E}_t^s + \nabla \times \left[\hat{n}\left(\hat{n} \cdot \nabla \times \frac{c_\circ}{2}\int_0^t e^{\frac{c_\circ}{r}(\tau - t)}\mathcal{E}^s \, d\tau\right)\right] + \nabla_t\left(\nabla \cdot \frac{c_\circ}{2}\int_0^t e^{\frac{c_\circ}{r}(\tau-t)}\mathcal{E}_t^s \, d\tau\right). \tag{15}$$

Substitution of (15) into (12), recognizing that for a linear vector expansion the last integral in (15) is zero, separation of the incident and total fields and subsequent rearrangement leads to the FETD/ABC matrix equation

$$\mathbf{T}_F\frac{d^2}{dt^2}\mathbf{e}(t) + (\mathbf{R}_F + \mathbf{R}_A)\frac{d}{dt}\mathbf{e}(t) + \mathbf{S}_F\mathbf{e}(t) + \mathbf{Q}_A\int_0^t e^{\frac{c_\circ}{r}(\tau-t)}\mathbf{e}(\tau) \, d\tau = \mathbf{v}(t) \tag{16}$$

where the elements of the ABC matrix $\mathbf{R}_A$ are given by

$$R_{A_{m,n}} = \frac{1}{\eta_\circ}\int_S (\mathbf{w}_m \cdot \mathbf{w}_{nt})\, dS \tag{17}$$

the elements of the ABC matrix $\mathbf{Q}_A$ are given by

$$Q_{A_{m,n}} = \frac{c_\circ}{2\mu_\circ}\int_S [(\hat{n}\cdot\nabla\times\mathbf{w}_m)(\hat{n}\cdot\nabla\times\mathbf{w}_n)]\, dS \tag{18}$$

and the elements of the excitation vector $\mathbf{v}(t)$ are given by

$$\begin{aligned} v_m(t) = &-\frac{1}{\mu_\circ}\int_S \mathbf{w}_m\cdot(\hat{n}\times\nabla\times\mathcal{E}^i)\, dS \\ &+\frac{1}{\eta_\circ}\int_S\left(\mathbf{w}_m\cdot\frac{\partial}{\partial t}\mathcal{E}_t^i\right)dS + \frac{c_\circ}{2\mu_\circ}\int_0^t e^{\frac{c_\circ}{r}(\tau-t)} \\ &\times\int_S (\hat{n}\cdot\nabla\times\mathbf{w}_m)(\hat{n}\cdot\nabla\times\mathcal{E}^i)\, dS\, d\tau. \end{aligned} \tag{19}$$

Note that the first order ABC (Sommerfeld radiation condition) formulation can be recovered from (16) by ignoring the term involving $\mathbf{Q}_A$ and the last integral in (19).

IV. Time-Stepping Methods

The FETD/ABC matrix equation of (16) possesses the basic structure given by

$$\begin{aligned} &\mathbf{T}\frac{d^2}{dt^2}\mathbf{e}(t) + \mathbf{R}\frac{d}{dt}\mathbf{e}(t) + \mathbf{S}\mathbf{e}(t) \\ &\quad + \mathbf{Q}\int_0^t e^{\frac{c}{r}(\tau-t)}\mathbf{e}(\tau)\, d\tau = \mathbf{v}(t). \end{aligned} \tag{20}$$

The solution for the time-domain total electric field involves stepping this integro-differential equation forward in time given a set of initial conditions. This is accomplished by discretizing (20) in time steps of δt. Two discretization schemes are presented here. The first is the backward Euler method, which approximates the first derivative in time with a simple backward difference [21]. This yields the following solution for $\mathbf{e}^j$, the vector of expansion coefficients at time $t = j\delta t$ given by:

$$\begin{aligned} \mathbf{e}^j = &\left[\frac{1}{\delta t^2}\mathbf{T} + \frac{1}{\delta t}\mathbf{R} + \mathbf{S} + \delta t\mathbf{Q}\right]^{-1} \\ &\cdot\left[\mathbf{v}^j + \left[\frac{2}{\delta t^2}\mathbf{T} + \frac{1}{\delta t}\mathbf{R}\right]\mathbf{e}^{j-1} - \frac{1}{\delta t^2}\mathbf{T}\mathbf{e}^{j-2}\right. \\ &\left. - \delta t\mathbf{Q}\sum_{i=1}^{j-1} e^{\frac{c_\circ}{r}(i-j)\delta t}\mathbf{e}^i\right]. \end{aligned} \tag{21}$$

Note that the integral has been approximated with step integration.

The second discretization scheme is the Θ method [2], [22], which is based on a local temporal quadratic approximation of the electric field coefficients. Application of the Θ method to (20) while approximating the integral with step integration yields

$$\begin{aligned} \mathbf{e}^j = &\left[\frac{1}{\delta t^2}\mathbf{T} + \frac{1}{\delta t}\left(2\Theta_1 + \frac{1}{2}\right)\mathbf{R} + (2\Theta_2 + \Theta_1)\mathbf{S}\right. \\ &\left. + \delta t(2\Theta_2 + \Theta_1)\mathbf{Q}\right]^{-1} \\ &\cdot\left[(2\Theta_2 + \Theta_1)\mathbf{v}^j - (4\Theta_2 - 1)\mathbf{v}^{j-1} + (2\Theta_2 - \Theta_1)\mathbf{v}^{j-2}\right. \\ &+\left[\frac{2}{\delta t^2}\mathbf{T} + \frac{4\Theta_1}{\delta t}\mathbf{R} + (4\Theta_2 - 1)\mathbf{S}\right. \\ &\left. + \delta t(4\Theta_2 - 1 - e^{-\frac{c_\circ}{r}\delta t}[2\Theta_2 + \Theta_1])\mathbf{Q}\right]\mathbf{e}^{j-1} \\ &-\left[\frac{1}{\delta t^2}\mathbf{T} + \frac{1}{\delta t}\left(2\Theta_1 - \frac{1}{2}\right)\mathbf{R} + (2\Theta_2 - \Theta_1)\mathbf{S}\right]\mathbf{e}^{j-2} \\ &\quad + \delta t[(2\Theta_2 - \Theta_1) - (4\Theta_2 - 1)e^{-\frac{c_\circ}{r}\delta t} \\ &\quad \left. + (2\Theta_2 + \Theta_1)e^{-2\frac{c_\circ}{r}\delta t}]\mathbf{Q}\sum_{i=1}^{j} e^{\frac{c_\circ}{r}(i-j)\delta t}\mathbf{e}^i\right] \end{aligned} \tag{22}$$

where Θ_1 and Θ_2 are scalar parameters.

In order to obtain a solution, a discretization scheme must possess the property of stability. Stability ensures that errors in the solution such as roundoff do not grow without bound. It can be shown that the backward Euler scheme is unconditionally stable; that is, it is stable for all δt. The Θ method can be shown to be unconditionally stable for $\Theta_1 \geq 0$ and $\Theta_2 \geq \frac{1}{8}$. Appendix A provides a proof for these stability conditions.

In order to start a solution, initial conditions are needed. The initial conditions are that the fields are everywhere zero in V and, thus, $\mathbf{e}^0$ and $\mathbf{e}^{-1}$ are both chosen to be $\mathbf{0}$. Time stepping is terminated when all transients have sufficiently decayed. In the case of continuous wave excitation, the time history of $\mathbf{e}^j$ is converted to phasor form in order to get the far field at the frequency of the excitation. In the case of a Gaussian pulse excitation, the time-domain far field at a single point is computed from the time history of $\mathbf{e}^j$ and then the fast Fourier transform is used to obtain the far field over a band of frequencies. In the computer code, the inverses in (21) and (22) are not computed explicitly, but rather the conjugate gradient method for sparse matrices [23] is employed to compute $\mathbf{e}^j$.

V. Results

Five sets of results of FETD computations on an IRIS Indigo SGI workstation with a MIPS R4400 processor with a 150-MHz clock rate are presented here. The first set of results concern a comparison between FEFD and FETD. Fig. 1 shows the bistatic RCS for a 0.1-m-radius PEC sphere at 0.3 GHz for both FEFD and FETD and various mesh densities. It is noted that the FEFD and FETD curves match each other for each value of mesh density. Fig. 1 shows that FETD can produce the same results as FETD. Note also that a mesh density of 20 nodes/λ produces adequate results.

The second set of results concern the ABC order and distance. Figs. 2 and 3 show FETD computed backscatter radar cross section (RCS) for a 0.1-m-radius PEC sphere with the

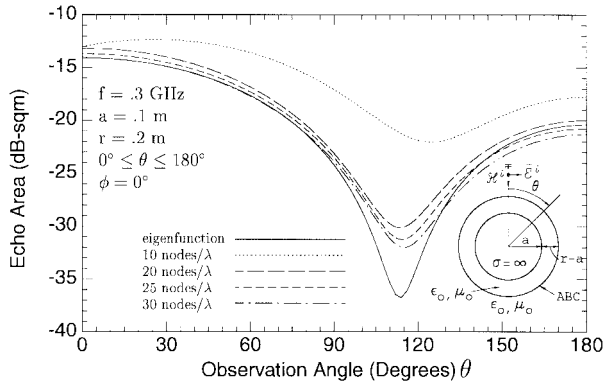

Fig. 1. FEFD and FETD backward Euler ($\delta t = .005$ ns) generated bistatic RCS ($\hat{\theta}\hat{\theta}$) in the $\phi = 0^\circ$ plane for a 0.1-m-radius PEC sphere with first-order ABC. (Both FEFD and FETD curves overlap.)

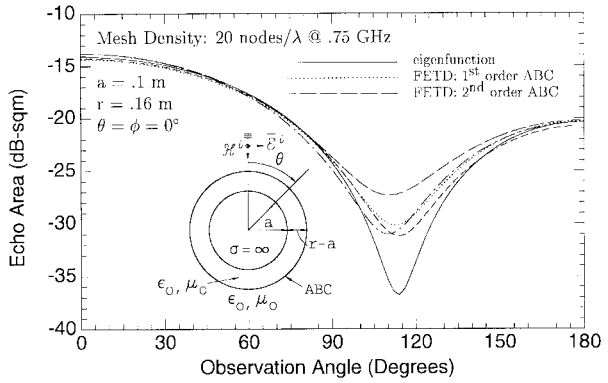

Fig. 2. FETD backward Euler ($\delta t = .005$ ns) generated monostatic RCS ($\hat{\theta}\hat{\theta}$) for a 0.1-m-radius PEC sphere with ABC radius of 0.16 m.

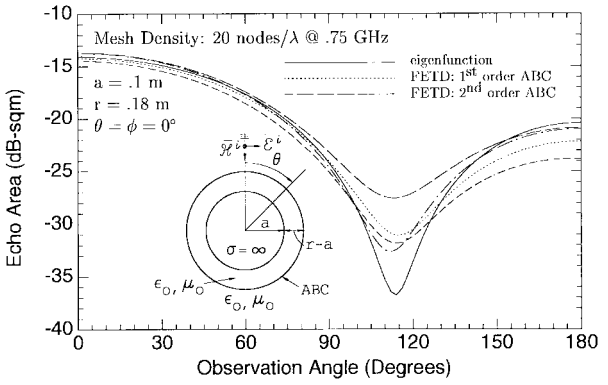

Fig. 3. FETD backward Euler ($\delta t = .005$ ns) generated monostatic RCS ($\hat{\theta}\hat{\theta}$) for a 0.1-m-radius PEC sphere with ABC radius of 0.18 m.

ABC boundary respectively located at 0.06 m and 0.08 m above the sphere surface. It can be seen that ABC distance is a critical factor in FETD computation. It can also be seen that the second-order ABC, as implemented in Section III, has the same level of performance as the first-order ABC.

The third set of results concerns the time-domain resistive boundary condition. Fig. 4 shows normal backscatter RCS for a 0.2-m-square resistive sheet of resistivity 200 Ω/□ as computed by FEFD and the moment method. There is

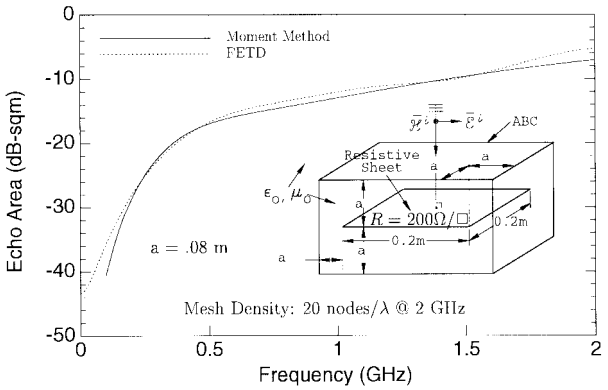

Fig. 4. Far-field backscatter ($\hat{\theta}\hat{\theta}$) for a 0.2 m square resistive sheet of $R = 200\ \Omega/\square$ with first-order ABC, Theta method with $\Theta_1 = 0$ and $\Theta_2 = 0.125$.

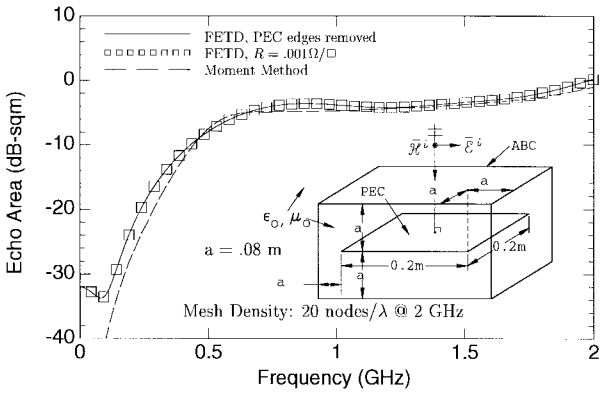

Fig. 5. Far-field backscatter ($\hat{\theta}\hat{\theta}$) for a 0.2-m square PEC sheet with first-order ABC, Θ method with $\Theta_1 = 0$ and $\Theta_2 = 0.125$.

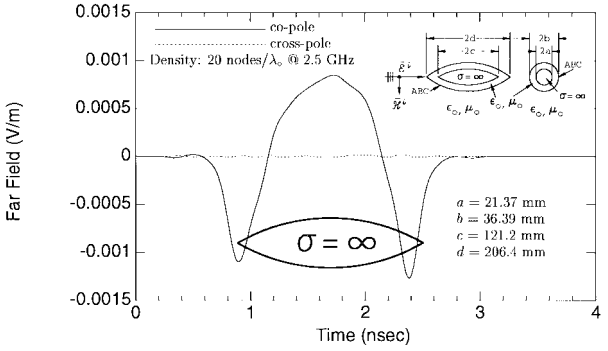

Fig. 6. Time-domain backscattered far fields for the ogive, with excitation incident along the main axis.

excellent agreement between the FEFD and moment method solutions. As a further check of the resistive boundary condition, backscatter RCS results for a PEC sheet of the same dimensions are shown in Fig. 5. Two FETD curves are displayed, one for the PEC edge unknowns removed and the other with the edges left in the mesh and the resistive boundary condition of 0.001 Ω/□ employed. As can be seen, both curves match each other and have good agreement with the moment method solution.

The fourth set of results concern a PEC ogive. Fig. 6 show FETD generated time-domain backscattered far fields for axial

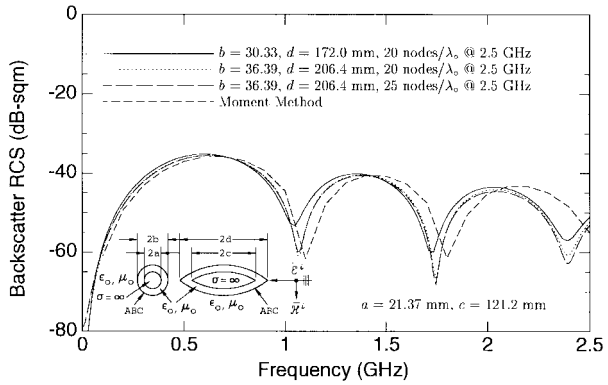

Fig. 7. Frequency-domain copole far field for the ogive, with excitation incident along the main axis.

TABLE I
Θ METHOD ($\Theta_1 = 0, \Theta_2 = 0.125$) FETD TIMING STATISTICS FOR .3-GHz CW EXCITATION FOR THE 0.1-m-RADIUS PEC SPHERE FORVARIOUS NUMBER OF EXTRAPOLATION POINTS FOR THE INITIAL CG GUESS VECTOR

Points	CPU Time (sec)
1	366
2	247
3	158
4	151
5	165

incidence. Superimposed over the copole far-field curve is an ogive twice its length in light nanoseconds. A Gaussian pulse was employed as the excitation and the returns from the front and back ends of the ogive are easily seen. However, the distance between the returns is a little shorter than expected. This is probably due to the coarseness of the mesh near the tips which has the effect of making the ogive appear smaller than it is. This coarseness is also probably the cause of the nonzero cross-pole return. Fig. 7 show frequency-domain axially backscattered RCS as computed by FETD for three meshes of the ogive and by the moment method. As can be seen, the FETD formulation is capable of producing reasonable RCS results for an object such as the PEC ogive.

The fifth and last set of results concern timing issues. It was found that the provision of the conjugate gradient algorithm at each time step with an initial guess vector greatly increased the speed of the FETD computation. The guess vector was computed by fitting a separate polynomial curve to each of the edge unknowns based on the behavior at the previous few time steps. The guess vector is then obtained from evaluating the polynomials at the present time step. As can be seen in Table I for the CW excitation and in Table II for the Gaussian pulse excitation, three-point extrapolation (using the time history for the last three time steps) is the best in terms of solution time and memory requirements. The major benefit of extrapolation for the initial guess vector is the excellent convergence characteristics acheived with the conjugate gradient algorithm (10–30 iterations per time step).

Three-point extrapolation was employed in a timing test based on problem size, the results of which are given in Fig. 8.

TABLE II
Θ METHOD ($\Theta_1 = 0, \Theta_2 = 0.125$) FETD TIMING STATISTICS FOR 1.25-GHz-BANDWIDTH GAUSSIAN PULSE EXCITATION FOR THE 0.1-m-RADIUS PEC SPHERE FOR VARIOUS NUMBER OF EXTRAPOLATION POINTS FOR THE INITIAL CG GUESS VECTOR

Points	CPU Time (sec)
1	498
2	384
3	306
4	312
5	302

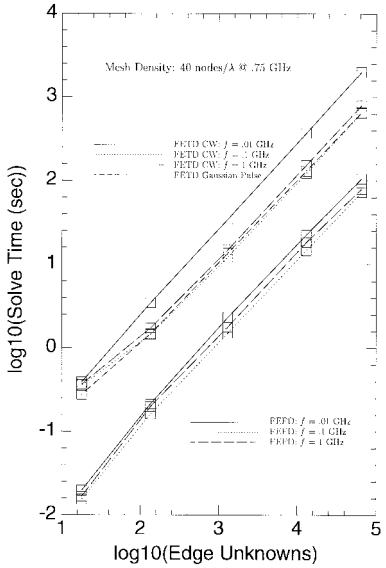

Fig. 8. Finite-element free-space bar calculation timing statistics.

The test geometry employed were five rectangular free-space bars with a cross section of 0.01 m by 0.01 m and lengths of 0.01, 0.1, 1, 10, and 50 m, with a broadside incident field. FEFD and FETD CW calculations were made at 0.01, 0.1, and 1 GHz. In the FETD CW case, 1.25 cycles were allowed to pass through the mesh before termination of the calculation and there were 200 time steps per cycle. As can be seen, FEFD is by far preferable time-wise to FETD CW for single frequency calculations. Also, there is little dependence on frequency as far as solution time is concerned. Also included in Fig. 8 are the timing statistics for an FETD Gaussian pulse calculation. In this case, the solution time is the time required for the bulk of the pulse to propagate through the mesh. As can be seen, the FETD Gaussian pulse approach produces a broad-band solution in roughly the same amount of time as a single FETD CW calculation. It is anticipated that the FETD pulse approach will be useful for resolving sharp variations in the RCS such as with high Q resonances, where many closely spaced frequency points would be required. Finally, Fig. 8 also suggests that FETD has a solve time of order N, where N is the number of edge unknowns in the finite-element mesh. In conclusion, memory requirements are generally the same for FEFD and FETD, the choice of algorithm depends upon the problem: FEFD for single-frequency applications and FETD

for broad-band applications. Note that as the unknown count becomes large, FEFD techniques have convergence concerns while none have been observed with this FETD technique.

VI. Conclusion

A FETD formulation based on the Helmholtz equation with a second-order ABC has been developed for 3-D material scatterers. It has been found that ABC boundary distance is a crucial factor in FETD RCS computation. The second-order ABC was found to work just as well as the first-order ABC. Excellent results were obtained for various PEC and resistive geometries. It was found that three-point polynomial extrapolation for the CG guess vector greatly improved solution time. Finally, FETD/ABC has been shown to have a potential for use in timely computation of RCS with sharp variations in a small frequency band as opposed to the conventional FEFD approach.

Appendix A

In order to obtain a solution, a discretization scheme must possess the property of stability. Stability ensures that errors in the solution such as roundoff do not grow without bound. For the first-order ABC, it can be shown that the backward Euler scheme is unconditionally stable; that is, stable for any δt. Likewise, for the first-order ABC, the Θ method can be shown to be unconditionally stable for $\Theta_1 \geq 0$ and $\Theta_2 \geq 1/8$. In both cases, the property of unconditional stability can be easily shown through the bilinear transformation. The stability of the discretization schemes for the second-order ABC requires similar treatment and is outlined here.

Following is verification of the Θ method stability condition for the first-order ABC with a backward Euler scheme.

Application of the Z transform to (21) yields

$$(\mathbf{T}+\delta t\mathbf{R}+\delta t^2\mathbf{S})z^2-(2\mathbf{T}+\delta t\mathbf{R})z + \mathbf{T}+\delta t^3\mathbf{Q}z^2\sum_{i=1}^{j}(e^{\frac{c_0\delta t}{r}})^{(i-j)}=0. \tag{23}$$

The above summation for large time $(j\to\infty)$ reduces to

$$\lim_{j\to\infty}\sum_{i=1}^{j}(e^{\frac{c_0\delta t}{r}})^{(i-j)}=\sum_{k=0}^{\infty}(e^{\frac{c_0\delta t}{r}})^{-k}=\frac{(e^{\frac{c_0\delta t}{r}})}{(e^{\frac{c_0\delta t}{r}})-1}. \tag{24}$$

Insertion of the resulting summation expression into the z-transformed equation yields

$$\begin{aligned}&(e^{\frac{c_0\delta t}{r}}[\mathbf{T}+\delta t\mathbf{R}+\delta t^2\mathbf{S}+\delta t^3\mathbf{Q}])z^3\\&\quad-([\mathbf{T}+\delta t\mathbf{R}+\delta t^2\mathbf{S}]+e^{\frac{c_0\delta t}{r}}[2\mathbf{T}+\delta t\mathbf{R}])z^2\\&\quad+([2\mathbf{T}+\delta t\mathbf{R}]+e^{\frac{c_0\delta t}{r}}\mathbf{T})z-\mathbf{T}=0.\end{aligned} \tag{25}$$

Replacement of z with the bilinear transformation of $\frac{1+w}{1-w}$ yields

$$\begin{aligned}&(e^{\frac{c_0\delta t}{r}}[\mathbf{T}+\delta t\mathbf{R}+\delta t^2\mathbf{S}+\delta t^3\mathbf{Q}])(1+w)^3\\&\quad-([\mathbf{T}+\delta t\mathbf{R}+\delta t^2\mathbf{S}]+e^{\frac{c_0\delta t}{r}}[2\mathbf{T}+\delta t\mathbf{R}])\\&\quad\times(1+w)^2(1-w)+([2\mathbf{T}+\delta t\mathbf{R}]+e^{\frac{c_0\delta t}{r}}\mathbf{T})\\&\quad\times(1+w)(1-w)^2-\mathbf{T}(1-w)^3=0.\end{aligned} \tag{26}$$

$$\begin{aligned}&(e^{\frac{c_0\delta t}{r}}[\mathbf{T}+\delta t\mathbf{R}+\delta t^2\mathbf{S}+\delta t^3\mathbf{Q}])(w^3+3w^2+3w+1)\\&\quad-([\mathbf{T}+\delta t\mathbf{R}+\delta t^2\mathbf{S}]+e^{\frac{c_0\delta t}{r}}[2\mathbf{T}+\delta t\mathbf{R}])\\&\quad\times(w^3+w^2-w-1)\\&\quad+([2\mathbf{T}+\delta t\mathbf{R}]+e^{\frac{c_0\delta t}{r}}\mathbf{T})(w^3-w^2-w+1)\\&\quad-\mathbf{T}(w^3-3w^2+3w-1)=0.\end{aligned} \tag{27}$$

The above polynominal in w can be separated into four inequalites for each power of w to yield

$$\begin{aligned}&e^{\frac{c_0\delta t}{r}}[4\mathbf{T}+2\delta t\mathbf{R}+\delta t^2\mathbf{S}+\delta t^3\mathbf{Q}]\\&\quad+[4\mathbf{T}+2\delta t\mathbf{R}+\delta t^2\mathbf{S}]\geq 0\end{aligned} \tag{28}$$

$$\begin{aligned}&e^{\frac{c_0\delta t}{r}}[4\mathbf{T}+4\delta t\mathbf{R}+3\delta t^2\mathbf{S}+3\delta t^3\mathbf{Q}]\\&\quad+[-4\mathbf{T}+\delta t^2\mathbf{S}]\geq 0\end{aligned} \tag{29}$$

$$\begin{aligned}&e^{\frac{c_0\delta t}{r}}[2\delta t\mathbf{R}+3\delta t^2\mathbf{S}+3\delta t^3\mathbf{Q}]\\&\quad-\left[2\delta t\mathbf{R}+\delta t^2\mathbf{S}\right]\geq 0\end{aligned} \tag{30}$$

and

$$e^{\frac{c_0\delta t}{r}}[\delta t^2\mathbf{S}+\delta t^3\mathbf{Q}]-\delta t^2\mathbf{S}\geq 0. \tag{31}$$

These four inequalities are true for any δt since the matrices $\mathbf{R}$, $\mathbf{S}$, $\mathbf{T}$, and $\mathbf{Q}$ are all positive definite which results in unconditional stability.

Following is the verification of the Θ method stability condition for the second-order ABC with a backward Euler scheme.

Application of the Z transform to (22) yields

$$\begin{aligned}&\left(\mathbf{T}+\left[2\Theta_1+\frac{1}{2}\right]\delta t\mathbf{R}+[2\Theta_2+\Theta_1]\delta t^2\mathbf{S}\right)z^2\\&\quad-(2\mathbf{T}+4\Theta_1\delta t\mathbf{R}+[4\Theta_2-1]\delta t^2\mathbf{S})z\\&\quad+\left(\mathbf{T}+\left[2\Theta_1-\frac{1}{2}\right]\delta t\mathbf{R}+[2\Theta_2-\Theta_1]\delta t^2\mathbf{S}\right)\\&\quad+\delta t^3\mathbf{Q}([2\Theta_2+\Theta_1]z^2-4\Theta_1 z\\&\quad+[2\Theta_2-\Theta_1]\sum_{i=1}^{j}(e^{\frac{c_0\delta t}{r}})^{(i-j)}=0.\end{aligned} \tag{32}$$

Insertion of the previous summation reduction yields

$$\begin{aligned}&e^{\frac{c_0\delta t}{r}}\left(\mathbf{T}+\left[2\Theta_1+\frac{1}{2}\right]\delta t\mathbf{R}+[2\Theta_2+\Theta_1]\delta t^2\mathbf{S}\right.\\&\quad\left.+[2\Theta_2+\Theta_1]\delta t^3\mathbf{Q}\right)z^3\\&\quad-\left(\mathbf{T}+\left[2\Theta_1+\frac{1}{2}\right]\delta t\mathbf{R}+[2\Theta_2+\Theta_1]\delta t^2\mathbf{S}\right.\\&\quad\left.+e^{\frac{c_0\delta t}{r}}(2\mathbf{T}+4\Theta_1\delta t\mathbf{R}+[4\Theta_2-1]\delta t^2\mathbf{S}+4\Theta_1\delta t^3\mathbf{Q})\right)z^2\\&\quad+\left(2\mathbf{T}+4\Theta_1\delta t\mathbf{R}+[4\Theta_2-1]\delta t^2\mathbf{S}\right.\\&\quad\left.+e^{\frac{c_0\delta t}{r}}\left(\mathbf{T}+\left[2\Theta_1-\frac{1}{2}\right]\delta t\mathbf{R}+[2\Theta_2-\Theta_1]\delta t^2\mathbf{S}\right.\right.\\&\quad\left.\left.+[2\Theta_2-\Theta_1]\delta t^3\mathbf{Q}\right)\right)z\\&\quad-\left(\mathbf{T}+\left[2\Theta_1-\frac{1}{2}\right]\delta t\mathbf{R}+[2\Theta_2-\Theta_1]\delta t^2\mathbf{S}\right)=0.\end{aligned} \tag{33}$$

Application of the same bilinear transformation as before and separating for each power of w yields

$$e^{\frac{c_0\delta t}{r}}(4\mathbf{T}+8\Theta_1\delta t\mathbf{R}+[8\Theta_2-1]\delta t^2\mathbf{S}+4[\Theta_2+\Theta_1]\delta t^3\mathbf{Q}) + (4\mathbf{T}+8\Theta_1\delta t\mathbf{R}+[8\Theta_2-1]\delta t^2\mathbf{S})\geq 0 \quad (34)$$

$$e^{\frac{c_0\delta t}{r}}(4\mathbf{T}+[8\Theta_1+2]\delta t\mathbf{R}+[5\Theta_2+4\Theta_1-1]\delta t^2\mathbf{S} + [6\Theta_2+8\Theta_1]\delta t^3\mathbf{Q})+(-4\mathbf{T}+[-8\Theta_1+2]\delta t\mathbf{R} \times[-8\Theta_2+4\Theta_1+1]\delta t^2\mathbf{S})\geq 0 \quad (35)$$

$$e^{\frac{c_0\delta t}{r}}(2\delta t\mathbf{R}+[4\Theta_1+1]\delta t^2\mathbf{S}+4\Theta_2\delta t^3\mathbf{Q}) - (2\delta t\mathbf{R}+[4\Theta_1-1]\delta t^2\mathbf{S})\geq 0 \quad (36)$$

and

$$e^{\frac{c_0\delta t}{r}}[\delta t^2\mathbf{S}+[4\Theta_2-4\Theta_1]\delta t^3\mathbf{Q}]-\delta t^2\mathbf{S}\geq 0. \quad (37)$$

These four inequalities are true for any δt when $\Theta_1 \geq 0$, $\Theta_2 \geq 1/8$, and $\Theta_2 \geq \Theta_1$ since the matrices $\mathbf{R}$, $\mathbf{S}$, $\mathbf{T}$, and $\mathbf{Q}$ are all positive definite.

REFERENCES

[1] A. Taflove and E. Brodwin, "Numerical solution of steady-state electromagnetic scattering problems using the time-dependent Maxwell's equations," *IEEE Trans. Microwave Theory Tech.*, vol. 23, pp. 623–630, Aug. 1975.

[2] O. C. Zienkiewicz and R. L. Taylor, *The Finite Element Method*, 4th ed. New York: McGraw-Hill, 1988.

[3] J. D'Angelo and I. Mayergoyz, "Finite element methods for the solution of RF radiation and scattering problems," *Electromagn.*, vol. 10, pp. 177–199, 1990.

[4] J. Lee, R. Lee, and A. Cangellaris, "Time-domain finite element methods," *IEEE Trans. Antennas Propagat.*, vol. 45, pp. 430–442, Mar. 1997.

[5] P. Silvester and R. Ferrari, *Finite Elements for Electrical Engineers*, 2nd ed. Cambridge, U.K.: Cambridge Univ. Press, 1990.

[6] J. Lee, "WETD—A finite element time-domain approach for solving Maxwell's equations," *IEEE Microwave Guided Wave Lett.*, vol. 4, pp. 11–13, Jan. 1994.

[7] D. Dibben and R. Metaxas, "Time domain finite element analysis of multimode microwave applicators," *IEEE Trans. Magn.*, vol. 32, pp. 942–945, May 1996.

[8] J. Berenger, "A perfectly matched layer for the absorption of electromagnetic waves," *J. Computat. Phys.*, vol. 114, no. 2, pp. 185–200, Oct. 1994.

[9] W. Chew and W. Weedon, "A 3D perfectly matched medium from modified Maxwell's equations with stretched coordinates," *Microwave Opt. Technol. Lett.*, vol. 7, no. 13, pp. 599–604, Sept. 1994.

[10] J. Wang, "On 'edge'-based finite elements and method of moments solutions of electromagnetic scattering and coupling," Ph.D. dissertation, Univ. Akron, OH, May 1992.

[11] N. Wang and A. Dominek, "FEM/ABC and FEM/BEM techniques for electromagnetic scattering from three-dimensional termination structures," Rep. 723224-8, Grant NAG3-1000, NASA Lewis Res. Ctr., ElectroSci. Lab., Ohio State Univ., Columbus, May 1994.

[12] B. Engquist and A. Majda, "Absorbing boundary conditions for the numerical simulation of waves," *Math. Computat.*, vol. 31, no. 139, pp. 629–651, July 1977.

[13] J. Webb and V. Kanellopoulos, "Absorbing boundary conditions for the finite element solution of the vector wave equation," *Microwave Opt. Technol. Lett.*, vol. 2, no. 10, pp. 370–372, Oct. 1989.

[14] G. Mur, "Absorbing boundary conditions for the finite-difference approximation of the time-domain electromagnetic field equations," *IEEE Trans. Electromagn. Compat.*, vol. 23, pp. 377–382, Nov. 1981.

[15] H. Ali and G. Costache, "Finite-element time-domain analysis of axisymmetrical radiators," *IEEE Trans. Antennas Propagat.*, vol. 42, pp. 272–275, Feb. 1994.

[16] K. Mahadevan and R. Mittra, "Radar cross section computation of inhomogeneous scatterers using edge-based finite element methods in frequency and time domains," *Radio Sci.*, vol. 28, no. 6, pp. 1181–1193, Nov./Dec. 1996.

[17] K. Komisarek, "An investigation of FETD/ABC methods for computation of scattering from three dimensional material objects," Ph.D. dissertation, Ohio State Univ., Columbus, 1997.

[18] R. Luebbers, D. Steich, and K. Kunz, "FDTD calculation of scattering from frequency-dependent materials," *IEEE Trans. Antennas Propagat.*, vol. 41, pp. 1249–1257, Sept. 1993.

[19] M. Barton and Z. Cendes, "New vector finite elements for three-dimensional magnetic field computation," *J. Appl. Phys.*, vol. 61, no. 8, pp. 3919–3921, Apr. 1987.

[20] A. Bossavit and I. Mayergoyz, "Edge-elements for scattering problems," *IEEE Trans. Magn.*, vol. 25, pp. 2816–2821, July 1989.

[21] S. S. Kuo, *Computer Applications of Numerical Methods*. Reading, MA: Addison-Wesley, 1972.

[22] W. L. Wood, *Practical Time-Stepping Schemes*. Oxford, U.K.: Clarendon, 1990.

[23] W. H. Press, S. A. Teukolsky, W. T. Vetterling, and B. P. Flannery, *Numerical Recipes in FORTRAN*, 2nd ed. Cambridge, U.K.: Cambridge Univ. Press, 1994.

Kenneth S. Komisarek was born on September 7, 1968. He received the B.S.E.E. and M.S.E.E. degrees from the University of New Hampshire, Durham, in 1991 and 1992, respectively, and the Ph.D. degree in electrical engineering from The Ohio State University, Columbus, in 1997.

From 1993 to 1997, he was employed at the ElectroScience Laboratory, Ohio State University, as a Graduate Research Associate. Since 1997 he has been employed as a Senior Engineer at Raytheon Systems Company Radar Design Center, Sudbury, MA. His research interests include theoretical and experimental electromagnetic radiation and scattering and the development and application of numerical methods for electromagnetic problems.

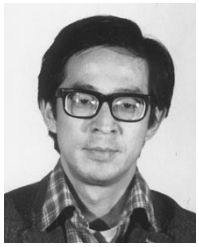

Nan N. Wang was born in Szechuang, China, on September 3, 1945. He received the B.S.E.E. degree in electrical engineering form Taiwan Cheng Kung University, Tainan, Taiwan, in 1965, the M.S.E.E. degree in electrical engineering from the University of Mississippi, in 1968, and the Ph.D. degree in electrical engineering form The Ohio State University, Columbus, in 1974.

From 1970 to 1999, he was engaged in research on antenna and scattering problems at the ElectroScience Laboratory, Department of Electrical Engineering, The Ohio State University.

Allen K. Dominek was born on April 8, 1957. He received the B.S.E.E. and M.S.E.E. degrees from the University of North Dakota, Grand Forks, in 1978 and 1980, respectively, and the Ph.D. degree in electrical engineering from The Ohio State University, Columbus, in 1984.

From 1985 to 1997, he was with ElectroScience Laboratory, Ohio State University, as a Senior Research Associate and Research Scientist. Since 1997 he has been with Analytic Designs, Inc., Columbus, OH. His research interests include electromagnetic radiation and scattering from both experimental and analytical foundations.

Raiford Hann, photograph and biography not available at the time of publication.